# Tuning the Relative Concentration Ratio of Bulk Defects to Surface Defects in TiO2 Nanocrystals Leads to High Photocatalytic Efficiency

7 AUTHORS, INCLUDING:

Yuanzhi Li
Wuhan University of Technology
60 PUBLICATIONS   1,936 CITATIONS

SEE PROFILE

Pengfei Fang
Wuhan University
80 PUBLICATIONS   1,160 CITATIONS

SEE PROFILE

Xiujian Zhao
Wuhan University of Technology
456 PUBLICATIONS   7,126 CITATIONS

SEE PROFILE

# Tuning the Relative Concentration Ratio of Bulk Defects to Surface Defects in TiO₂ Nanocrystals Leads to High Photocatalytic Efficiency

Ming Kong,[†] Yuanzhi Li,*[,†] Xiong Chen,[†] Tingting Tian,[†] Pengfei Fang,[‡] Feng Zheng,[‡] and Xiujian Zhao[†]

[†]State Key Laboratory of Silicate Materials for Architectures, Wuhan University of Technology, 122 Luoshi Road, Wuhan 430070, P.R. China

[‡]Department of Physics, Wuhan University, Luojia Hill, Wuhan 430072, P.R. China

**S** *Supporting Information*

**ABSTRACT:** TiO₂ nanocrystals with tunable bulk/surface defects were synthesized and characterized with TEM, XRD, BET, positron annihilation, and photocurrent measurements. The effect of defects on photocatalytic activity was studied. It was found for the first time that decreasing the relative concentration ratio of bulk defects to surface defects in TiO₂ nanocrystals could significantly improve the separation efficiency of photogenerated electrons and holes, thus significantly enhancing the photocatalytic efficiency.

The photoactivation of TiO₂ has received enormous attention from scientists and engineers in the past decade, owing to its important applications in photocatalysis for environmental cleanup, solar cells, clean H₂ energy production, antimicrobial activity, and more.[1] The widely accepted photoactivation mechanism is as follows: Upon UV excitation of TiO₂ by light absorption with energy equal to or greater than the band gap of the semiconductor, electrons are excited from the valence band to the conduction band. The photogenerated electrons (e) and holes (h) migrate from bulk to surface, where electrons reduce adsorbed electron acceptor (e.g., O₂) and holes oxidize adsorbed donor species (e.g., organic species or hydroxyl). Thus, e−h recombination is in competition with charge transfer to adsorbed species. Mechanistic studies clearly demonstrate that the majority of photogenerated electrons and holes recombine, resulting in a quite moderate photoactivation efficiency.[2−5] The e−h recombination occurs in bulk defects or on surface defects.[6] Therefore, it is of scientific and technological significance to characterize the defects and reveal the effect of defects on the photoactivation as well as surface reactivity and adsorption, which may lead to breakthroughs in the rational design of novel materials for specific practical applications. The significance has triggered broad interest and intensive studies of the defect chemistry of TiO₂. The defects (e.g., oxygen vacancies) in TiO₂ have been theoretically studied with first-principles calculations[7−9] and experimentally studied by scanning tunneling microscopy (STM),[10−14] electron paramagnetic resonance spectroscopy (EPR),[15,16] time-resolved photoluminescence spectroscopy (PL),[17,18] etc. The effect of defects in anatase and rutile on the electronic properties,[7] reactivity, and adsorption−desorption with H₂O, CO₂, and O₂[10−14] has been reported. These studies have mostly focused on the effect of surface or subsurface defects, which plays a decisive role in adsorption and surface reactivity.

The effect of surface/bulk defects on photocatalysis is still unclear. Surface defects serve as charge carrier traps as well as adsorption sites where the charge transfer to adsorbed species can prevent the e−h recombination, whereas bulk defects only act as charge carrier traps where e−h recombines. In principle, both surface and bulk defects play very important roles in the photoactivation processes. Among the techniques for characterization of defects, STM, one of most powerful techniques, can provide direct images of surface or subsurface defects.[10−14] However, STM cannot provide information about bulk defects. Positron annihilation is a well-established technique to study defects in materials. It is able to give information about the size, type, and relative concentration of various defects/vacancies, even at the ppm level.[19−22] Herein, TiO₂ nanocrystals with tunable bulk/surface defects were synthesized and then characterized with positron annihilation and photocurrent measurements. It was found for the first time that decreasing the relative concentration ratio of bulk defects to surface defects in the TiO₂ nanocrystals could significantly improve the e−h separation efficiency, thus significantly enhancing the photocatalytic efficiency.

A sample of TiO₂ nanocrystals with a higher ratio of bulk defects to surface defects was prepared by vapor-induced hydrothermal hydrolysis at 120 °C, using titanium butoxide as precursor, followed by photothermocatalytic treatment (denoted as TiO₂-120, see Supporting Information).[23] Another sample of TiO₂ nanocrystals with a lower ratio of bulk defects to surface defects was prepared by the same procedure except at 180 °C (denoted as TiO₂-180). The third sample of TiO₂ nanocrystals, with the lowest ratio of bulk defects to surface defects, was prepared by calcination of TiO₂-180 at 480 °C for 3 h (denoted as TiO₂-480). TEM images of TiO₂-120 reveal that it is composed of 7.8−14.9 nm nanoparticles, each of which is a single anatase crystal with exposed facet {101} (Figure 1a,b). TiO₂-180 is composed of 9.2−23.5 nm nanoparticles with single anatase crystal structure with exposed facet {101} (Figure 1c,d). Calcination of TiO₂-180 at 480 °C does not change its single anatase crystal structure. TiO₂-480 is characteristic of 11.5−24.5 nm single anatase crystals with exposed facet {101} (Figure 1e,f). XRD analysis (Figure S1) reveals that all of the TiO₂ samples are indexed to the pure anatase structures (JCPDS-89-4921). The average crystal size of TiO₂-120, TiO₂-180, and TiO₂-480, determined by using the Scherrer formula ($L = 0.89\lambda/\beta \cos\theta$) is 11.2, 13.4, and 15.5 nm, respectively, which is in agreement
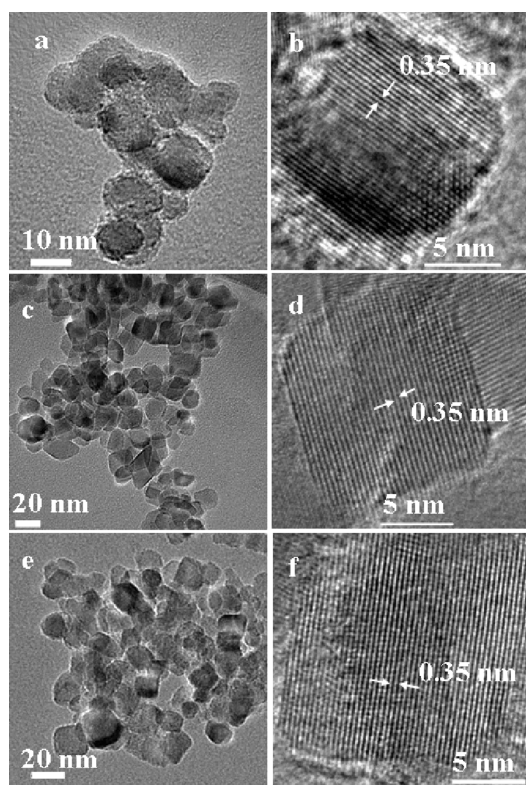
**Figure 1.** TEM and HRTEM images of the samples of TiO$_2$ nanocrystals: TiO$_2$-120 (a,b), TiO$_2$-180 (c,d), and TiO$_2$-480 (e,f).

**Table 1. Positron Lifetime and Relative Intensities of the TiO$_2$ Samples**

| sample | $\tau_1$ (ps) | $\tau_2$ (ps) | $\tau_3$ (ns) | $I_1$ (%) | $I_2$ (%) | $I_3$ (%) | $I_1/I_2$ |
|---|---|---|---|---|---|---|---|
| TiO$_2$-120 | 183.8 | 371.3 | 2.0933 | 50.123 | 49.636 | 0.2416 | 1.01 |
| TiO$_2$-180 | 180.2 | 381.6 | 3.1126 | 42.259 | 57.547 | 0.1941 | 0.73 |
| TiO$_2$-480 | 178.5 | 362.5 | 7.6097 | 31.015 | 68.84 | 0.1456 | 0.45 |
| TiO$_2$(P25) | 189.3 | 385.2 | 2.8907 | 30.59 | 69.125 | 0.2846 | 0.44 |

with the TEM observation. The BET surface area of TiO$_2$-120, TiO$_2$-180, and TiO$_2$-480 is 192.4, 120.0, and 100.9 m$^2$/g, respectively.

The defects in the TiO$_2$ samples were characterized by positron annihilation. Table 1 shows three positron lifetime components, $\tau_1$, $\tau_2$, and $\tau_3$, with relative intensities $I_1$, $I_2$, and $I_3$ for TiO$_2$-120, TiO$_2$-180, and TiO$_2$-480. The longest component ($\tau_3$) for all samples was probably due to the annihilation of orthopositronium atoms formed in the large voids present in the material.[19−22] The shortest one ($\tau_1$) is generally attributed to the free annihilation of positrons in defect-free crystal.[20,24,25] However, in disordered systems, smaller vacancies (like monovacancies, etc.) or shallow positron traps (like oxygen vacancies in ZnO) decrease the average electron density,[20,24] thus resulting in elongation of $\tau_1$. In the present case, $\tau_1$ for TiO$_2$-120 and TiO$_2$-180 is 183.8 and 180.2 ps, respectively, both of which are larger than that of the reported TiO$_2$ crystal (178 ps).[26] This result suggests the presence of defects with small size in the TiO$_2$ nanocrystals.

The second lifetime components ($\tau_2$) for TiO$_2$-120, TiO$_2$-180, and TiO$_2$-480 are much larger than their corresponding
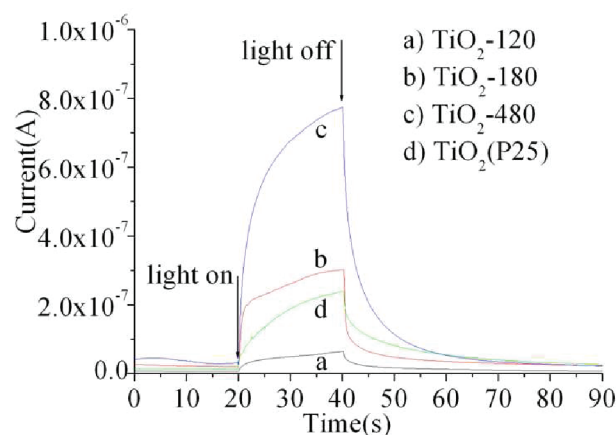


**Figure 2.** Transient response of the photocurrent for the TiO$_2$ samples under the UV irradiation in air.

shortest lifetime components ($\tau_1$). This indicates that $\tau_2$ arises from positrons trapped by larger size defects such as oxygen vacancy clusters (i.e., dimers, trimers, or larger),[27] since in such larger size defects the average electron density is lower than that in small size defects, thus decreasing the annihilation rate, and consequently increasing the positron lifetime.[22,27] The small size defects mainly exists in the bulk of the TiO$_2$ samples, while the larger size defects mainly locate on the surface or subsurface of the TiO$_2$ samples, as the formation of titania nanocomposite (e.g., AgI/TiO$_2$) does not lead to an obvious change of $\tau_1$ but results in a considerable evolution of $\tau_2$.[28]

Besides the lifetime of the positron, its relative intensity ($I$) provides information on the relative concentration of the defects.[19−22,27] The ratio of $I_1$ to $I_2$ ($I_1/I_2$) for TiO$_2$-120 is 1.01, indicating that the concentration of small size bulk defects is almost same as that of larger size surface defects. The relative concentration ratio of bulk defects to surface defects ($C_{bd}/C_{sd}$) can be tuned by controlling the synthesis conditions. Increasing the temperature of hydrothermal hydrolysis from 120 to 180 °C leads to a decrease of $I_1/I_2$ from 1.01 to 0.73, indicating that it results in a decrease of $C_{bd}/C_{sd}$. Furthermore, calcination of TiO$_2$-180 at 480 °C can further decrease $C_{bd}/C_{sd}$, which is evidenced by the decrease of $I_1/I_2$ from 0.73 to 0.45 after the calcination (Table 1). The lowest $I_1/I_2$ of TiO$_2$-480, together with its lowest $\tau_1$ (178.5 ps), which is almost same as that of the reported TiO$_2$ crystal (178.0 ps),[26] reveals that a higher hydrothermal synthesis temperature followed by calcination at 480 °C results in anatase nanocrystals with an almost perfect bulk crystal structure. For comparison, Table 1 also lists the result of positron annihilation for a mixed-phase Degussa TiO$_2$(P25) sample. The $I_1/I_2$ (0.44) of TiO$_2$(P25) is almost same as that of TiO$_2$-480, indicating very low concentration of small size bulk defects in TiO$_2$(P25).

It is widely accepted that the e−h separation efficiency plays a decisive role in the photocatalytic reaction:[6] the higher the photocurrent is, the higher the e−h separation efficiency is, and thus the higher the photocatalytic activity is. Therefore, the photocurrent of the TiO$_2$ samples was measured under UV irradiation (Figure 2A). Among the TiO$_2$ samples, TiO$_2$-120, with the highest $C_{bd}/C_{sd}$, exhibits the lowest photocurrent, which is attributed to the recombination of most photogenerated charge carriers in the bulk defects. Decreasing $C_{bd}/C_{sd}$ in the TiO$_2$ nanocrystal leads to a significant increase in the e−h

16415

dx.doi.org/10.1021/ja207826q |*J. Am. Chem. Soc.* 2011, 133, 16414–16417
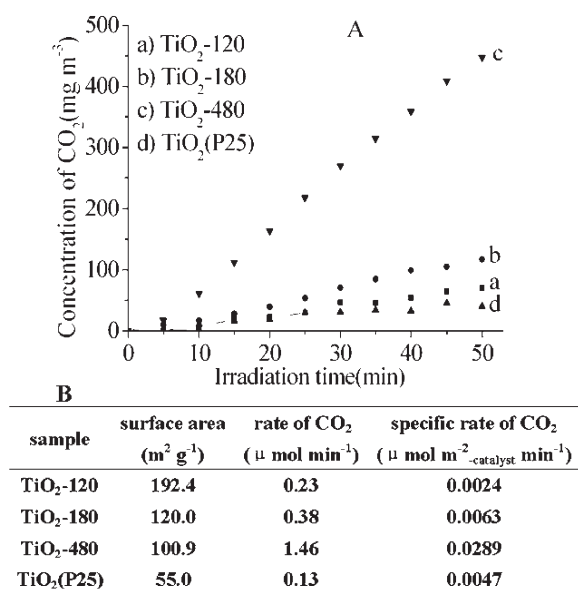
**Figure 3.** Time course of $CO_2$ produced for benzene photocatalytic oxidation (A) and the corresponding specific rate of $CO_2$ production (B) on the $TiO_2$ catalysts under UV irradiation.

separation efficiency. The maximum photocurrent of $TiO_2$-180 with lower $C_{bd}/C_{sd}$ is 4.8 times higher than that of $TiO_2$-120. $TiO_2$-480 exhibits the highest photocurrent because it has the lowest $C_{bd}/C_{sd}$, which significantly decreases the recombination of photogenerated charge carriers in bulk. The maximum photocurrent of $TiO_2$-480 is 12.7, 2.7 times higher than those of $TiO_2$-120 and $TiO_2$-180, respectively. These results demonstrate that the e—h separation efficiency for the $TiO_2$ nanocrystals can be controlled considerably by tuning the relative concentration ratio of bulk defects to surface defects.

It is well known that mixed-phase $TiO_2$(P25) shows higher e—h separation efficiency; thus, it exhibits higher photocatalytic activity than either pure phase alone due to the transfer of photogenerated electrons from rutile to anatase.[29] Surprisingly, $TiO_2$(P25) shows much lower e—h separation efficiency than $TiO_2$-480, evidenced by the observation that the maximum photocurrent of the latter is 3.3 times higher than that of the former. Positron annihilation characterization indicates that the $C_{bd}/C_{sd}$ of $TiO_2$(P25) is almost the same as that of $TiO_2$-480 (Table 1). However, there are electron-trapping sites in the distorted interfacial region due to the strain that exists at the interface between rutile and anatase nanoparticles in $TiO_2$-(P25).[29] Positron annihilation in the present work confirms the existence of interfacial defects in $TiO_2$(P25), as its $\tau_1$ (189.3 ps) is larger than $\tau_1$ for $TiO_2$-120 (183.8 ps), $TiO_2$-180 (180.2 ps), and $TiO_2$-480 (178.5 ps) (Table 1). However, positron annihilation could not distinguish interfacial defects from bulk defects in $TiO_2$(P25). The interfacial electron-trapping sites may act as recombination centers, resulting in a decrease in the e—h separation efficiency as compared to that of the pure anatase nanocrystal with perfect bulk crystal structure (e.g., $TiO_2$-480).

The effect of defects on the photocatalytic activity of $TiO_2$ nanocrystals was investigated by evaluating the rate of $CO_2$ production from the gas-phase photocatalytic oxidation of benzene on the $TiO_2$ catalysts under the irradiation of a 125-W Hg lamp. As shown in Figure 3A, all of the $TiO_2$ samples of anatase nanocrystals exhibit a much higher total $CO_2$ production

rate than $TiO_2$(P25), a widely used benchmark photocatalyst. The total $CO_2$ production rates of $TiO_2$-120, $TiO_2$-180, and $TiO_2$-480 are 1.8, 2.9, and 11.2 times higher than that of $TiO_2$(P25), respectively. As the $TiO_2$ catalysts have different specific surface areas, their specific rates of $CO_2$ production (per unit surface area of catalyst), which represents the intrinsic photocatalytic efficiency of $TiO_2$, are compared (Figure 3B). $TiO_2$-120, with the highest $C_{bd}/C_{sd}$, exhibits the lowest specific $CO_2$ production rate. Decreasing $C_{bd}/C_{sd}$ leads to a significant enhancement in the photocatalytic activity. The specific rate of $CO_2$ production of $TiO_2$-180 is 2.6 and 1.3 times higher than those of $TiO_2$-120 and $TiO_2$(P25), respectively. $TiO_2$-480, with the lowest $C_{bd}/C_{sd}$, exhibits the highest photocatalytic activity, and its specific $CO_2$ production rate is 12.0, 4.6, and 6.1 times higher than those of $TiO_2$-120, $TiO_2$-180, and $TiO_2$(P25), respectively. The significant photocatalytic enhancement is due to the considerable enhancement of e—h separation efficiency that is achieved by decreasing $C_{bd}/C_{sd}$ of the $TiO_2$ nanocrystals, as discussed above.

Several strategies have been reported for improving the photocatalytic efficiency of $TiO_2$: (1) The first strategy involves controlling the exposed facets (e.g., {001}) of the $TiO_2$ crystal, which has received intensive interest very recently.[30−34] But there is discrepancy among the reported results: some researchers reported that the {001} facets with a higher surface energy exhibited a higher photocatalytic activity than the energetically stable {101} facets,[30−32,33a] while other researchers reported that the {101} facets showed a higher photocatalytic activity than {001} facets.[33b,34] (2) The second strategy takes advantage of the effects of multiple scattering and slow photons in the $TiO_2$ photonic crystal.[35,36] (3) The third strategy involves forming a rutile/anastase junction to improve the separation of the photogenerated e—h pairs.[37,38] However, our present evidence shows that the unavoidable interfacial defects at the rutile/anastase junction accelerate e—h recombination, thus counteracting the beneficial effect of charge transfer between rutile and anatase. (4) The fourth strategy involves increasing the specific surface area through preparing various photocatalysts of mesoporous and macro-/mesoporous $TiO_2$.[39−41] But it is difficult to increase the intrinsic specific photocatalytic efficiency of $TiO_2$ by this strategy. The present strategy of improving photocatalytic efficiency by tuning the surface/bulk defects of $TiO_2$ nanocrystals is one of most efficient approaches, as evidenced by the very high photocatalytic enhancement factor as compared to $TiO_2$(P25).

In summary, both surface and bulk defects in $TiO_2$ nanocrystals play very important roles in photocatalysis. Decreasing the relative concentration ratio of bulk defects to surface defects in $TiO_2$ nanocrystals significantly improves the e—h separation efficiency, thus significantly enhancing the photocatalytic efficiency. The findings of this work provide fundamental insight into the role of surface/bulk defects in photoactivation and open up a novel strategy for significantly improving photocatalytic efficiency through controlling the surface/bulk defects of photocatalysts. We believe that the strategy may also be applicable to other photocatalysts, such as ZnO, $SnO_2$, etc.

## ■ ASSOCIATED CONTENT

**ⓢ Supporting Information.** Experimental details and XRD patterns of the $TiO_2$ nanocrystals. This material is available free of charge via the Internet at http://pubs.acs.org.

## ■ AUTHOR INFORMATION

**Corresponding Author**
liyuanzhi66@hotmail.com

## ■ ACKNOWLEDGMENT

## ■ REFERENCES

(1) (a) Chen, X. B.; Mao, S. S. *Chem. Rev.* **2007**, *107*, 2891. (b) Chen, X.; Liu, L.; Yu, P. Y.; Mao, S. S. *Science* **2011**, *331*, 746.

(2) Serpone, N.; Lawless, D.; Khairutdinov, R.; Pelizzetti, E. *J. Phys. Chem.* **1995**, *99*, 16655.

(3) Leytner, S.; Hupp, J. T. *Chem. Phys. Lett.* **2000**, *330* (3−4), 231.

(4) Bahnemann, D. W.; Hilgendorff, M.; Memming, R. *J. Phys. Chem. B* **1997**, *101*, 4265.

(5) Tang, J. W.; Durrant, J. R.; Klug, D. R. *J. Am. Chem. Soc.* **2008**, *130*, 13885.

(6) (a) Linsebigler, A. L.; Lu, G. Q.; Yates, J. T., Jr. *Chem. Rev.* **1995**, *95*, 735. (b) Thompson, L.; Yates, J. T., Jr. *Chem. Rev.* **2006**, *106*, 4428.

(7) Mattioli, G.; Filippone, F.; Alippi, P.; Bonapasta1, A. A. *Phys. Rev. B.* **2008**, *78*, 241201.

(8) Na-Phattalung, S.; Smith, M. F.; Kim, K.; Du, M. H.; Wei, S. H.; Zhang, S. B.; Limpijumnong, S. *Phys. Rev. B* **2006**, *73*, 125205.

(9) Cheng, H. Z.; Selloni, A. *Phys. Rev. B* **2009**, *79*, 092101.

(10) (a) He, Y. B.; Dulub, O.; Cheng, H. Z.; Selloni, A.; Diebold, U. *Phys. Rev. Lett.* **2009**, *102*, 106105. (b) He, Y. B.; Tilocca, A.; Dulub, O.; Selloni, A.; Diebold, U. *Nat. Mater.* **2009**, *8*, 585.

(11) Gong, X. Q.; Selloni, A.; Batzill, M.; Diebold, U. *Nat. Mater.* **2006**, *5*, 665.

(12) Lee, J.; Sorescu, D. C.; Deng, X. Y. *J. Am. Chem. Soc.* **2011**, *133*, 10066.

(13) Lira, E.; Wendt, S.; Huo, P.; Hansen, J.; Streber, R.; Porsgaard, S.; Wei, Y. Y.; Bechstein, R.; Lægsgaard, E.; Besenbacher, F. *J. Am. Chem. Soc.* **2011**, *133*, 6529.

(14) Cui, X. F.; Wang, B.; Wang, Z.; Huang, T.; Zhao, Y.; Yang, J. L.; Hou, J. G. *J. Chem. Phys.* **2008**, *129*, 044703.

(15) Li, M.; Hebenstreit, W.; Diebold, U.; Tyryshkin, A. M.; Bowman, M. K.; Dunham, G. G.; Henderson, M. A. *J. Phys. Chem. B* **2000**, *104*, 4944.

(16) Berger, T.; Sterrer, M.; Diwald, O.; Knozinger, E.; Panayotov, D.; Thompson, T. L.; Yates, J. T., Jr. *J. Phys. Chem. B* **2005**, *109*, 6061.

(17) Wang, X. L.; Feng, Z. C.; Shi, J. Y.; Jia, G. Q.; Shen, S.; Zhou, J.; Li, C. *Phys. Chem. Chem. Phys.* **2010**, *12*, 7083.

(18) Iijima, K.; Goto, M.; Enomoto, S.; Kunugita, H.; Ema, K.; Tsukamoto, M.; Ichikawa, N.; Sakama, H. *J. Lumin.* **2008**, *128*, 911.

(19) Chakraverty, S.; Mitra, S.; Mandal, K.; Nambissan, P. M. G.; Chattopadhyay, S. *Phys. Rev. B* **2005**, *71*, 024115.

(20) Dutta, S.; Chattopadhyay, S.; Jana, D.; Banerjee, A.; Manik, S.; Pradhan, S. K.; Sutradhar, M.; Sarkar, A. *J. Appl. Phys.* **2006**, *100*, 114328.

(21) Sachdeva, A.; Chavan, S. V.; Goswami, A.; Tyagi, A. K.; Pujari, P. K. *J. Solid State Chem.* **2005**, *178*, 2062.

(22) Dannefaer, S.; Bretagnon., T.; Kerr, D. *J. Appl. Phys.* **1993**, *74*, 884.

(23) Li, Y. Z.; Huang, J. C.; Peng, T.; Xu, J.; Zhao, X. J. *ChemCatChem* **2010**, *2*, 1082.

(24) Sanyal, D.; Banerjee, D.; De, U. *Phys. Rev. B* **1998**, *58*, 15226.

(25) de la Cruz, R. M.; Pareja, R.; Gonzalez, R.; Boatner, L. A.; Chen, Y. *Phys. Rev. B* **1992**, *45*, 6581.

(26) Murakami, H.; Onizuka, N.; Sasaki, J.; Thonghai, N. *J. Mater. Sci.* **1998**, *33*, 5811.

(27) Liu, X. W.; Zhou, K. B.; Wang, L.; Wang, B. Y.; Li, Y. D. *J. Am. Chem. Soc.* **2009**, *131*, 3140.

(28) Sun, W.; Li, Y. Z.; Shi, W. Q.; Zhao, X. J.; Fang, P. F. *J. Mater. Chem.* **2011**, *21*, 9263.

(29) Hurum, D. C.; Gray, K. A.; Rajh, T.; Thurnauer, M. C. *J. Phys. Chem. B* **2005**, *109*, 977.

(30) Wu, B.; Guo, C.; Zheng, N.; Xie, Z.; Stucky, G. D. *J. Am. Chem. Soc.* **2008**, *130*, 17563.

(31) Han, X.; Kuang, Q.; Jin, M.; Xie, Z.; Zheng, L. *J. Am. Chem. Soc.* **2009**, *131*, 3152.

(32) Amano, F.; Yasumoto, T.; Prieto-Mahaney, O. O.; Uchida, S.; Shibayama, T.; Ohtani, B. *Chem. Commun.* **2009**, 2311.

(33) (a) Yang, H. G.; Liu, G.; Qiao, S. Z.; Sun, C. H.; Jin, Y. G.; Smith, S. C.; Zou, J.; Cheng, H. M.; Lu, G. Q. *J. Am. Chem. Soc.* **2009**, *131*, 4078. (b) Pan, J.; Liu, G.; Lu, G. Q.; Cheng, H. M. *Angew. Chem., Int. Ed.* **2011**, *50*, 2133.

(34) Tachikawa, T.; Wang, N.; Yamashita, S.; Cui, S.-C.; Majima, T. *Angew. Chem., Int. Ed.* **2010**, *49*, 8593.

(35) Li, Y. Z.; Kunitake, T.; Fujikawa, S. *J. Phys. Chem. B* **2006**, *110*, 13000.

(36) Chen, J. I. L.; von Freymann, G.; Choi, S. Y.; Kitaev, V.; Ozin, G. A. *Adv. Mater.* **2006**, *18*, 1915.

(37) Di Paola, A.; Bellardita, M.; Ceccato, R.; Palmisano, L.; Parrino, F. *J. Phys. Chem. C* **2009**, *113*, 15166.

(38) Kawahara, T.; Konishi, Y.; Tada, H.; Tohge, N.; Nishii, J.; Ito, S. *Angew. Chem., Int. Ed.* **2002**, *41*, 2811.

(39) Yu, J. C.; Zhang, L. Z.; Yu, J. G. *Chem. Mater.* **2002**, *14*, 4647.

(40) Peng, T.; Zhao, D.; Dai, K.; Shi, W.; Hirao, K. *J. Phys. Chem. B* **2005**, *109*, 4947.

(41) Yu, J. G.; Su, Y. R.; Cheng, B. *Adv. Funct. Mater.* **2007**, *17*, 1984.